



Published in final edited form as:

Ann Biomed Eng. 2019 January ; 47(1): 60–74. doi:10.1007/s10439-018-02122-y.

Development of a Functionally Equivalent Model of the Mitral Valve Chordae Tendineae Through Topology Optimization

Amir H. Khalighi¹, Bruno V. Rego¹, Andrew Drach¹, Robert C. Gorman², Joseph H. Gorman III², and Michael S. Sacks¹

¹James T. Willerson Center for Cardiovascular Modeling and Simulations, Institute for Computational Engineering and Sciences, Department of Biomedical Engineering, The University of Texas at Austin, Austin, TX, USA

²Gorman Cardiovascular Research Group, Department of Surgery, Perelman School of Medicine, University of Pennsylvania, Philadelphia, PA, USA

Abstract

Ischemic mitral regurgitation (IMR) is a currently prevalent disease in the US that is projected to become increasingly common as the aging population grows. In recent years, image-based simulations of mitral valve (MV) function have improved significantly, providing new tools to refine IMR treatment. However, clinical implementation of MV simulations has long been hindered as the *in vivo* MV chordae tendineae (MVCT) geometry cannot be captured with sufficient fidelity for computational modeling. In the current study, we addressed this challenge by developing a method to produce functionally equivalent MVCT models that can be built from the image-based MV leaflet geometry alone. We began our analysis using extant micron-resolution 3D imaging datasets to first build anatomically accurate MV models. We then systematically simplified the native MVCT structure to generate a series of synthetic models by consecutively removing key anatomic features, such as the thickness variations, branching patterns, and chordal origin distributions. In addition, through topology optimization, we identified the minimal structural complexity required to capture the native MVCT behavior. To assess the performance and predictive power of each synthetic model, we analyzed their performance by comparing the mismatch in simulated MV closed shape, as well as the strain and stress tensors, to ground-truth MV models. Interestingly, our results revealed a substantial redundancy in the anatomic structure of native chordal anatomy. We showed that the closing behavior of complete MV apparatus under normal, diseased, and surgically repaired scenarios can be faithfully replicated by a functionally equivalent MVCT model comprised of two representative papillary muscle heads, single strand chords, and a uniform insertion distribution with a density of 15 insertions/cm². Hence, even though the complete sub-valvular structure is mostly missing in *in vivo* MV images, we believe our approach will allow for the development of patient-specific complete MV models for surgical repair planning.

correspondence: Michael S. Sacks, msacks@ices.utexas.edu.

Conflict of Interest The authors declare no conflict of interest.

Keywords

Mitral Valve; Chordae Tendineae; Topology Optimization; Finite Element Analysis; Sub-valvular Apparatus

1 Introduction

The most recent statistics from the American Heart Association reported mitral valve (MV) disease as a common heart valve lesion in the US,⁵ afflicting more than 4 million Americans, with up to 350,000 new cases annually.⁵⁵ The most prevalent MV disorder, mitral regurgitation (MR), occurs at a frequency of 1.7%, ranging from 0.5% in the 18–44 age group to 9.3% among the elderly (age > 75 years).³⁴ Moreover, from more than 700,000 Americans who suffer heart attacks annually, over one-third of the surviving patients develop ischemic MR (IMR) within a month of infarction.⁹

As a prime example of functional complexity in living systems, the MV is a bi-leaflet structure suspended at the mitral annulus, and supported by thin collagenous structures called the MV chordae tendineae (MVCT) that connect the MV leaflets to the papillary muscles (PMs).³¹ The MVCT and PMs together are often referred to as the MV “sub-valvular apparatus” and play a critical role in the MV competence as well as the left ventricular (LV) geometry and function.³⁵ Most MV pathologies, IMR in particular, are accompanied by morphological and structural changes to the valve including annular dilation and flattening, in addition to posterior leaflet tethering.^{7,11,24}

To treat patients who suffer from moderate to severe IMR, MV repair and replacement are widely practiced, yet there has been an ongoing debate for more than two decades over which is the superior strategy.^{50,57,1,32} Numerous retrospective studies initially advocated MV repair over replacement as the preferred IMR treatment,^{15,8,21} however, recent randomized trials have cast significant doubt on the superiority of repair.^{51,20} In addition to the unknown optimal treatment, natural anatomic variations, different disease progression paths, and patient-specific tissue remodeling simultaneously impact the MV’s response to repair, which further obscures surgery outcomes and subsequently complicates treatment planning.^{42,48}

Computational modeling of the MV provides unique insights into valve function and disease as well as allowing for explorations within a range of treatment options that cannot be practically achieved via animal studies or clinical trials.^{54,41,3,42,48} In particular, image-based computational studies have advanced remarkably in recent years to more accurately simulate MV biomechanics.^{30,45,37} For instance, Zhang et al. developed a semi-automated framework to build patient-specific MV models from transesophageal echocardiography (TEE) images using machine learning and biomechanical models.⁵⁸ They applied their pipeline on 15 imaging datasets from 14 patients and demonstrated the accuracy of their approach to infer modeling parameters such as leaflet material properties. In another study, Gao et al. developed a coupled MV-LV model based on cardiac magnetic resonance imaging (MRI) data, which allowed them to simulate cardiac function over half of the cardiac cycle.¹⁹ While these studies have rigorously addressed some of the key challenges in *in vivo* MV

modeling, developing models strictly from clinical imaging data to faithfully predict MV surgeries remains an open-ended problem.

The inherent limitations of the clinical imaging modalities like real-time 3D echocardiography (rt-3DE) have long hampered the development of high-fidelity MV models on a patient-specific basis (Figure 1). More specifically, although *in vivo* imaging of the MV leaflets has improved significantly in the past decade, the MVCT anatomy remains largely unresolvable in current clinical imaging setups.¹² Therefore, most previous studies that attempted to perform image-based simulations of the MV relied on prescribing MVCT primarily based on *ex vivo* knowledge of chordal anatomy.^{38,39,56,52,40,33,53,36} However, given the intrinsic complexity and intra-patient variability of MVCT, MV models with prescribed chordal geometry suffer from low patient-specific precision and subsequently lack sufficient predictive power.¹³

In our previous investigation of the MVCT, we analyzed the geometric attributes of ten ovine MVs (Figure 2), which demonstrated significant regularities and suggested MVCT templates can be developed for a group of valves.²⁶ Such templates could then provide a generic substitute for the missing patient-specific MVCT structure based on population-representative approximations. However, acquiring large datasets to elucidate the population-level anatomic details of human MVCT using high-resolution imaging modalities such as micro-computed tomography (micro-CT) and MRI is prohibitively expensive and laborintensive.²² Most importantly, there is also no guarantee that such MVCT templates based on *population-averaged geometric attributes* provide predictive models to simulate the *patient-specific MV function*. Further, personalizing templates is a laborious task, prone to intractable inaccuracies that may negatively affect the fidelity of final models.² We believe these major challenges greatly disadvantage developing a template-based approach to build personalized MVCT models with reliable predictive power.

In the present study, we sought to establish a framework to build geometrically tractable, functionally equivalent models of the MVCT. To this end, we used our detailed knowledge of the MVCT to perform a functional characterization of the MV chordal structure and develop a functionally equivalent MVCT model through topology optimization. The rationale behind our approach originates from the Occam's razor principle to avoid unnecessarily sophisticated models in favor of more efficient solutions that deliver specific objectives. In this investigation, the main objective in developing functionally equivalent MVCT models was to reproduce the response of the native chordal structure for the purpose of predictive MV closure simulations under dilated (i.e. IMR-like) and repaired conditions. We believe that our work overcomes a significant challenge to ultimately adopt computational modeling of the MV in surgery simulations and hence treatment planning.

2 Materials and Methods

2.1 Geometry acquisition

We used extant *in vitro* imaging data from our previous studies to develop MV models. The details of our experimental setup, imaging protocols, and data processing algorithms have

been thoroughly reported in the literature.^{28,14,6} In brief, micro-CT images of three excised ovine MVs were acquired at both end-diastolic (fully open) and end-systolic (fully closed) states. Each specimen was imaged in normal, dilated, and surgically modified configurations that were simulated in a bench-top experimental setup. The obtained 3D images were first denoised using a curvature flow filter and then segmented using a standard thresholding scheme (see Khalighi²⁵). Further, a small angle light scattering technique was used to obtain the collagen fiber architecture (CFA) of the MV leaflet tissue.⁴⁹ To develop highly detailed geometric models, the leaflet and MVCT structures were extracted from fully open and fully closed images of the valve respectively. This enabled us to resolve the anatomic features of the MV structure with high precision and accuracy. The leaflets were analyzed in a multi-resolution framework that allowed controlling the level of detail and discretization using superquadric shape templates and sparse spectral analysis.²⁷ As for MVCT, curve-skeleton models enriched with continuous cross-sectional area (CSA) fields were developed that fully characterized and reconstructed the MVCT structure.²⁶

2.2 MVCT modeling

2.2.1 Model development—In this work, we developed a pipeline to generate MV models with synthetic, functionally equivalent MVCT structures based on our detailed knowledge of the native chordal anatomy (Figure 3). The models were built in the closed configuration of the valve following our previously established framework to build high-end MV models from imaging data.¹³ In brief, the leaflet geometry was hyperelastically warped from the open to the closed state using a marker-based morphing technique. Then, the chordal models were constructed in the same closed configuration and merged with the closed leaflet mesh. In addition to improved geometric resolution, this framework enabled us to calibrate the MV models efficiently and, in turn, enhance the predictive power when simulating valvular function under pathological conditions such as MR as well as surgically modified conditions such as AP repair. The specific steps of our numerical algorithms used to develop MV models have been described in detail in Drach et al.¹³

2.2.2 Functional characterization—To elucidate the functional impact of MVCT anatomic attributes, we developed a sequence of models by successively simplifying geometric features from the native MVCT anatomy (Figure 4). First, the locally varying CSA fields were replaced with the mean CSA value of the entire structure (Figure 4b). We then removed all the internal branching instances in the MVCT by directly connecting the chordal PM origins and leaflet insertions (Figure 4c). This model was further simplified by grouping the origins of the anterolateral and posteromedial PMs (Figure 4d). Each MVCT model in this ensemble isolated a key feature of the native chordal anatomy and thus performing simulations with these models enabled us to study how model accuracy is affected by the lack of knowledge regarding specific patient-specific native MVCT features.

2.2.3 Topology optimization—Following our functional characterization of the detailed native chordal anatomy, we studied functionally equivalent MVCT models in a topology optimization framework. The most simplified model studied in the 2.2.2 section was developed based on average origin locations and synthetic chordal strands. However, building that model still relied on the knowledge of native insertions. We thus homogenized

the chordal leaflet insertion sites by uniformly distributing the insertions across the leaflet surface (Figure 5a). The rationale behind this simplification was to completely eliminate the dependency of MVCT model development on information that cannot be acquired faithfully from low-resolution rt-3DE images. We then performed a topology optimization analysis on the MVCT model with combined origins and a uniform map of insertion locations.

In general, “topology optimization” is used in mechanical design to ascertain optimal shapes of a specific structure that fulfills a designated function.¹⁶ We adapted the same framework to develop geometrically tractable MVCT models that can effectively fulfill the function of native chordal anatomy for the purpose of organ-level simulations of the MV apparatus. Essentially, the goal in this part of the study was to search for an optimal density and distribution of single-strand chords with no branching that, when integrated with the leaflet structure, result in a predictive model of the valve’s closing behavior under dilated and repaired conditions.

The optimization was performed by iteratively removing a fraction of chords from the dense MVCT model with uniform insertions (Figure 5). Each iteration step consisted of first simulating the valve closure under normal conditions, then eliminating the chords in the bottom two deciles of the Cauchy stress histogram. The models were developed and tested successively until the onset of prolapse—when the synthetic chordal structures became overly sparse to support the leaflets during valve closure. We repeated the optimization algorithm to analyze the sensitivity of developed models to different step sizes in trimming the chords as well as the impact of mesh resolution for both leaflets and MVCT.

2.3 Finite element simulations

2.3.1 Geometry morphing—All the MVCT models developed in this study were originally constructed in the closed state. We thus were required to morph them to the open state prior to model calibration and closure simulations. As described in 2.2.1, to build models in the closed configuration, the leaflet mesh was initially morphed from the fully open to the fully closed state based on the methods established previously by Drach et al.¹³ In the present study, the inverse of this *closing* map was used to describe the *opening* boundary condition on the chordal insertion locations. As for the origins, displacement boundary conditions were prescribed based on the difference in the location of PMs in the imaging data from the fully open and fully closed states. Upon setting up the problem in a finite element (FE) framework, the opening simulations were performed with chords modeled as inextensible truss elements. Further details about the specifics of our approach to morph the MV constituent geometries between states can be found in our previous publications.^{26,27,13}

2.3.2 Model calibration—Morphing MV models from the fully closed to the fully open state only approximates the true open shape of MVCT when the chords are modeled as inextensible elements. Real chords undergo a substantial amount of strain, up to 10%, while deforming from their slacked shape in the fully open state to their stretched configuration in the fully closed state.^{10,46} To address this issue, we previously developed a calibration algorithm to infer the amount of compressive strain that needs to be applied in conjunction

with the opening simulations in order to predict the true open geometry of the MV.¹³ First, the MV model with inextensible chordal elements was pressurized to extract the true force distribution in the chords during the normal closure of the valve. The resulting force levels were then inverted based on the hyperelastic characteristics of MVCT to infer the strain that chords with real material properties undergo in the same setup. Lastly, to calibrate the MVCT, the inverse of this strain map was applied to the chords during opening simulations. This procedure ensured that the MV constructed in the closed state, then morphed to open state, and finally calibrated back to the closed state predicts the valvular function with guaranteed fidelity.¹³

2.3.3 Closure prediction—Our methodology to set up and perform predictive simulations of the MV closure has been previously described in detail.^{29,13} Briefly, the commercial FE software package ABAQUS Explicit was configured to use a nonlinear quasi-static solver with direct time integration and automatic time stepping. To build the computational mesh, first-order isoparametric triangular elements were used for the leaflet geometry and first-order isoparametric line elements were used for the MVCT. The mechanical behavior of leaflet tissue was simulated using a nearly incompressible, transversely isotropic structural model.^{17,59,43} The model is formulated as stiff fiber ensembles, embedded in a hydrated non-fibrous matrix material with the total strain energy function, Ψ , given by

$$\Psi = \Psi_f + \Psi_m = \int_{-\pi/2}^{\pi/2} \Gamma(\theta) \Psi_{ens} [E_{ens}(\theta)] d\theta + \frac{\mu_m}{2}(I_1 - 3) + p(J - 1) \quad (1)$$

In formulation 1, Ψ_f and Ψ_m are the effective fiber and matrix strain energies, respectively, Γ is the fiber orientation distribution function, Ψ_{ens} is the fiber ensemble strain energy density function, $E_{ens}(\theta) = \mathbf{N}^T(\theta) \mathbf{E} \mathbf{N}(\theta)$ is the ensemble fiber strain in the $\mathbf{N}(\theta)$ direction, $\mathbf{E} = (\mathbf{C} - \mathbf{I})/2$ is the tissue-level Green-Lagrange strain tensor, $\mathbf{C} = \mathbf{F}^T \mathbf{F}$ is the right Cauchy-Green deformation tensor, \mathbf{F} is the deformation gradient tensor, and \mathbf{I} is the identity tensor. In the second and third terms, μ_m is the matrix neo-Hookean material model constant, responsible for the bulk low-strain response, $I_1 = \text{trace}(\mathbf{C})$, $J = \det(\mathbf{F})$, and p is the Lagrange multiplier to enforce incompressibility. Using this constitutive relation and following the Fung pseudo-hyperelastic assumptions,¹⁸ the total second Piola-Kirchhoff stress tensor is then computed from

$$\mathbf{S}_L = \int_{-\pi/2}^{\pi/2} \Gamma(\theta) S_{ens} [E_{ens}(\theta)] \mathbf{N}(\theta) \otimes \mathbf{N}(\theta) d\theta + \mu_m (\mathbf{I} - C_{33} \mathbf{C}^{-1}) \quad (2)$$

where $C_{33} = 1/(C_{11}C_{22} - C_{12}^2)$ is the direct consequence of imposing incompressibility in planar tissues and $p = -\mu_m C_{33}$ is the Lagrange multiplier enforcing incompressibility. To simplify computations, we chose an exponential model to simulate the nonlinear fiber stress-strain response as

$$S_{ens}(E_{ens}) = \begin{cases} c_0 [\exp(c_1 E_{ens}) - 1] & \text{for } E_{ens} \leq E_{ub} \\ c_0 [\exp(c_1 E_{ub}) - 1] + c_0 c_1 \exp(c_1 E_{ub})(E_{ens} - E_{ub}) & \text{for } E_{ens} > E_{ub} \end{cases} \quad (3)$$

where c_0 and c_1 are the material constants and E_{ub} is the threshold fiber strain for full fiber recruitment. The material parameters used for simulations are reported in Drach et al.¹³ To model the mechanical behavior of MVCT, we used an incompressible isotropic hyper-elastic material relation following

$$S_{MVCT} = C_{10} [\exp(C_{01} E_{11}) - 1]. \quad (4)$$

In equation 4, $E_{11} = \frac{1}{2}(F_{11}^2 - 1)$ is the uniaxial strain in MVCT, and the material constants C_{10} and C_{01} were chosen as reported by Lee and colleagues.²⁹ The same material model was used for all the MVCT models developed and studied in this work.

2.4 Model comparisons

We compared the shape and kinematic measures of MV leaflets to quantitatively assess the performance of MV models with different chordal structures. All the studied models throughout this work shared the same leaflet geometry that provided a natural correspondence between them. The chordal part of models were excluded in the comparison since each model by design had a different MVCT topology. Essentially, the comparison criterion was based on the impact of each chordal model on the MV apparatus performance as a whole.

To facilitate model evaluations, we used the composite accuracy score (CAS), as originally used by Drach et al.¹³ This scalar score provides an effective metric to assess the accuracy of a specific model against ground-truth measurements. In this study, the native MV model was considered as the ground truth and all the other MVCT models were ranked based on how well they replicated the performance of the native structure under normal, dilated, and repaired conditions. CAS is computed using the explicit equation

$$CAS = \sum_k \left(\frac{\sqrt{\sum_i^N (q_{i,k} - \bar{q}_{i,k})^2}}{\sigma_{i,k}} \right) / dim(k), \quad k = \{S_{CC}, S_{RR}, E_{CC}, E_{RR}\}, \quad (5)$$

where k is index of the quantity of interest, i is the FE index and N is the total number of elements in the model, $q_{i,k}$ is the values of quantity of interest in the considered model, $\bar{q}_{i,k}$ is the quantity of interest in the reference model, $\sigma_{i,k}$ is the standard deviation of the quantity interest in the reference model.

3 Results

3.1 Functional characterization

To analyze the functional impact of native chordal features, we simulated MV closure under normal, dilated, and repaired conditions using systematically simplified models of the native MVCT (Figure 6). The results show that the local CSA variations, internal branching pattern, and the stochastic scatter of chordal origins on PMs only minimally affect the predictive power of MV models. We found that all models achieved at least 98% accuracy when comparing the results of closure simulations for the simplified MVCT models with the native model in terms of predicting shape as well as the stress and strain tensors. These findings imply that for the purpose of organ-level simulations of the MV, calibrated models of the MVCT comprised of only single strand chords with uniform CSA and combined origin locations can provide sufficiently accurate results.

3.2 Topology optimization

Building upon the insight that native chordal features have little impact on the *development* of predictive MV models, we studied structurally optimal MVCT models that can be developed in a topology optimization framework with no detailed knowledge of the native chordal anatomy. Interestingly, our results indicated that a simplified MVCT model with the same areal density of insertions as the native model is highly redundant to mimic the chordal role in the MV apparatus function (Figure 7). We further showed that the predictive power of this model to simulate altered states can be improved by trimming the structurally insignificant strands down to 15 ± 2 insertions/cm² on the leaflets surface (Figure 8). Comparing this finding to the 65.4 ± 4.2 insertions/cm² (mean \pm standard deviation, n=10), which is the native density of insertions,²⁶ suggests that over 75% of the native population of MVCT insertions can be eliminated with no significant loss in model performance.

3.3 Functionally equivalent models

Examining the evolution of insertion maps in our study of the MVCT through topology optimization showed no specific patterns, such as distinctly dense or significantly sparse insertion regions (Figure 5). Following this finding, we uniformly distributed the insertion locations for an optimal model (15 insertions/cm²) and performed additional FE closure simulations. The homogenization of insertion locations did not result in a significant decline in predictive power (Figure 9). We thus developed similar models for two more valves and assessed their performance under normal, dilated and repaired states (see Appendix for more details). The simulation results indicated that MVCT models with uniform insertion maps of an optimal density can reliably reproduce the performance of anatomically accurate chordal models (Table 1). More specifically, calibrated MVCT models comprised of two representative origin locations, single strand chords, and a uniform insertion map of 15 insertions/cm² can be used to mimic the behavior of the native chordal structure.

4 Discussion

4.1 Significance and novelty

Computational models of the MV provide an invaluable means to improve our understanding of the MV pathophysiology. Most notably, key questions regarding the functional significance of MV constituents, mechanobiological response of the valve tissue to disease, and development of more durable MV treatments are all within the scope of MV modeling based on biomechanical frameworks and computational algorithms. Our group has worked extensively on establishing a rigorous foundation to develop more reliable MV models based on *in vitro* studies.^{44,6,26,27,13,4} However, to be able to simulate patient-specific MV function, computational models need to be developed from clinical-quality imaging data. The current study is focused on addressing the issue that the complete MV geometry, and MVCT in particular, cannot be resolved via *in vivo* imaging with the sufficient fidelity required for *in silico* model development.

It is worth mentioning that we established a functional framework, rather than a strictly mathematical approach, to analyze the MVCT. Alternatively, advanced computational geometry frameworks like L-systems provide the foundation to reproduce tree-like structures such as MVCT.⁴⁷ However, in addition to overcoming the challenges of tailoring sophisticated algorithms to generate synthetic chords, there is no guarantee that such models, developed uninformed of MV function and based on geometric considerations only, allow for faithful patient-specific simulations of MV closure. We thus focused on the development of sufficiently detailed MVCT models that can be well calibrated to mimic the function of the native structure as opposed to building models that geometrically resemble the native chordal anatomy.

4.2 General findings and clinical implications

Three classes of MVCT models were developed and analyzed in this study. First, we developed an ensemble of MVCT models by successive simplification of the native chordal anatomy. Analyzing the performance of these models in predicting MV closure under normal, dilated, and repaired scenarios indicated that native chordal features such as area variations, branching patterns, and origin scatters are not crucial to developing predictive MVCT models for the purpose of organ-level simulations. We next performed a topology optimization analysis to investigate the role of native insertion locations (chordae-to-leaflet attachment sites) in simulating MV function. Interestingly, our results showed that the original areal density of insertion locations can be trimmed down to around one-fourth of the native density with no significant loss in predictive power. Lastly, we developed MVCT models with uniform insertion maps and an optimal density for three valves, which further demonstrated that functionally equivalent models of the chordal structure can be developed completely independently of the native MVCT anatomy.

To build personalized MVCT models, our pipeline requires only the leaflet geometries at the fully open and fully closed states of the valve, which eliminates the need for any *a priori* knowledge of the patient-specific chordal anatomy. This also implies that the time-consuming image processing step to extract MVCT from images is no longer required for

the MV model development. Further, the synthetic chords are initially constructed in the closed state, then undergo morphing to the open state, and finally get calibrated to the normal working condition of the MV. We showed that such models, when constructed with a sufficient density of chords and carefully calibrated, can reliably predict MV function under altered conditions such as dilation due to IMR and flat-ring AP in MV repair surgery. Ultimately, we believe that where the organ-level behavior of MV is of main concern, functionally equivalent MVCT models with simplified structures provide an efficient approach to circumvent the shortcomings of *in vivo* imaging modalities.

4.3 Insights into MV anatomy

Our study showed that biomechanical models with simplified structures can be developed to predict the closing behavior of the MV apparatus with high fidelity. While we acknowledge the limited scope of all computational models when simulating natural biological systems, we believe that some general insights can be drawn from the findings of present work. Most notably, our results suggest that the inherent complexity of MV chordal anatomy might be less directly tied to the functional efficacy of MVCT than commonly believed. We showed that “structurally simple” models of the MVCT can be developed to efficiently simulate the same effective function as the native chordal structure. This further implies that the intricate branching shape of MVCT may result from the biological factors governing the way valves are formed rather than optimally fulfilling specific physiological goals.

4.4 Limitations

Although we ultimately seek to develop MVCT models from clinical imaging data, in this study we worked with *ex vivo* MV images with micron-resolution accuracy. This choice of data source was necessary to provide a highly detailed model as the ground truth. Further, it allowed us to isolate the effect of different MVCT models on MV function while ensuring the other model constituents remain accurate. However, when working with *in vivo* data, local maps of thickness variations and the fiber architecture of leaflets cannot be acquired to the same level of accuracy.²³ We expect this lack of information to not affect developing functionally equivalent MVCT models as we have previously shown that high-fidelity MV models can be developed with lower-quality leaflet geometry and an average map of internal fiber architecture.¹³ It is also worth mentioning that we only focused on the MV function under dilated and repaired conditions in an acute sense, without considering the possible tissue remodeling effects. The MVCT models introduced in this study have only been validated to predict the MV closure in situations where the leaflet properties have not changed drastically compared to the healthy state of the tissue. Further investigations are required to elucidate the long-term effects of tissue remodeling and effective ways to adjust the computational MV models to account for new tissue characteristics.⁴²

4.5 Future directions

In the present study, leaflet geometries based on micro-CT imaging data were used to build the chordal models, however, we have previously shown that MV models with substantially lower leaflet accuracy still can be used effectively for the purpose of organ level MV simulations.¹³ This implies that our pipeline can be efficiently extended to develop personalized, synthetic MVCT models from clinical imaging data. The only major challenge

that needs to be addressed is the registration of leaflet geometries extracted from the end-diastolic and end-systolic time-points of the cardiac cycle. We believe mechanically penalized registration techniques within FE frameworks can be readily implemented to build correspondence between MV geometries from different states. Upon successful implementation of such techniques, synthetic MVCT models can be developed as proposed in this study to simulate MV repair surgery and develop optimal personalized treatments.

Acknowledgment

Research reported in this publication was supported by National Heart, Lung, and Blood Institute of the National Institutes of Health under award number R01-HL119297 to MSS and JHG, and the National Science Foundation grant no. DGE-1610403 to BVR.

Appendix

We performed our analysis presented in this work on 3 valves that were randomly selected from our extant dataset of micro-CT based MV models (Figure 10). The optimal models developed for all valves faithfully reproduced the effect of native chordal anatomy in terms of organ level simulations of the MV closure under normal, dialted, and repaired conditions (Figures 11 and 12). This consistency further indicates that functionally equivalent MVCT models allow performing predictive simulations of the MV apparatus to simulate clinically important conditions of the MV.

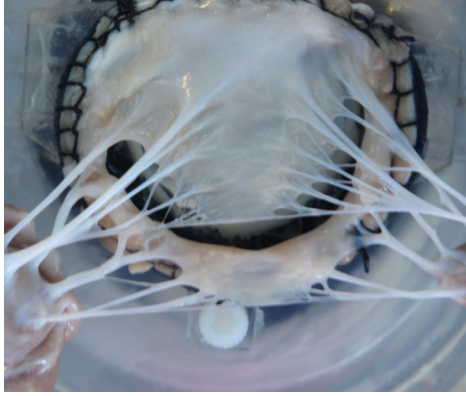
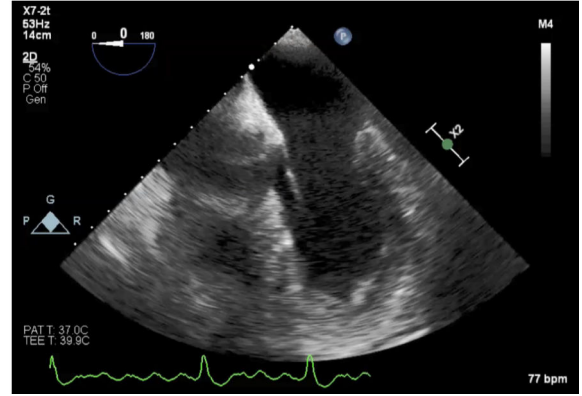
References

1. Acker MA, Parides MK, Perrault LP, Moskowitz AJ, Gelijns AC, Voisine P, Smith PK, Hung JW, Blackstone EH, Puskas JD et al. Mitral-valve repair versus replacement for severe ischemic mitral regurgitation. *New England Journal of Medicine* 370:23–32, 2014. [PubMed: 24245543]
2. Aggarwal A, Aguilar VS, Lee C-H, Ferrari G, Gorman JH, Gorman RC, and Sacks MS. Patient-specific modeling of heart valves: from image to simulation In: *International Conference on Functional Imaging and Modeling of the Heart*, pp. 141–149, Springer2013.
3. Ayoub S, Ferrari G, Gorman RC, Gorman JH, Schoen FJ, and Sacks MS. *Heart valve biomechanics and underlying mechanobiology*. *Comprehensive Physiology*, 2016.
4. Ayoub S, Lee C-H, Driesbaugh KH, Anselmo W, Hughes CT, Ferrari G, Gorman RC, Gorman JH, and Sacks MS. Regulation of valve interstitial cell homeostasis by mechanical deformation: implications for heart valve disease and surgical repair. *Journal of The Royal Society Interface* 14:20170580, 2017.
5. Benjamin EJ, Blaha MJ, Chiuve SE, Cushman M, Das SR, Deo R, Floyd J, Fornage M, Gillespie C, Isasi C et al. Heart disease and stroke statistics-2017 update: a report from the american heart association. *Circulation* 135:e146–e603, 2017. [PubMed: 28122885]
6. Bloodworth CH, Pierce EL, Easley TF, Drach A, Khalighi AH, Toma M, Jensen MO, Sacks MS, and Yoganathan AP. Ex vivo methods for informing computational models of the mitral valve. *Annals of biomedical engineering* 45:496–507, 2017. [PubMed: 27699507]
7. Bouma W, Lai EK, Levack MM, Shang EK, Pouch AM, Eperjesi TJ, Plappert TJ, Yushkevich PA, Mariani MA, Khabbaz KR et al. Preoperative threedimensional valve analysis predicts recurrent ischemic mitral regurgitation after mitral annuloplasty. *The Annals of thoracic surgery* 101:567–575, 2016. [PubMed: 26688087]
8. Braunberger E, Deloche A, Berrebi A, Fayssoil A, Celestin J, Meimoun P, Chatellier G, Chauvaud S, Fabiani J, and Carpentier A. Very long-term results (more than 20 years) of valve repair with carpentiers techniques in nonrheumatic mitral valve insufficiency. *Circulation* 104:I–8, 2001.

9. Bursi F, Enriquez-Sarano M, Nkomo VT, Jacobsen SJ, Weston SA, Meverden RA, and Roger VL. Heart failure and death after myocardial infarction in the community: the emerging role of mitral regurgitation. *Circulation* 111:295–301, 2005. [PubMed: 15655133]
10. Chen L, Yin FC, and May-Newman K. The structure and mechanical properties of the mitral valve leaflet-strut chordae transition zone. *Journal of biomechanical engineering* 126:244–251, 2004. [PubMed: 15179855]
11. Dal-Bianco JP, Beaudoin J, Handschumacher MD, and Levine RA. Basic mechanisms of mitral regurgitation. *Canadian Journal of Cardiology* 30:971–981, 2014. [PubMed: 25151282]
12. Dal-Bianco JP and Levine RA. Anatomy of the mitral valve apparatus: role of 2d and 3d echocardiography. *Cardiology clinics* 31:151–164, 2013. [PubMed: 23743068]
13. Drach A, Khalighi AH, and Sacks MS. A comprehensive pipeline for multi-resolution modeling of the mitral valve: Validation, computational efficiency, and predictive capability. *International journal for numerical methods in biomedical engineering*, 2017.
14. Drach A, Khalighi AH, ter Huurne FM, Lee C-H, Bloodworth C, Pierce EL, Jensen MO, Yoganathan AP, and Sacks MS. Population-averaged geometric model of mitral valve from patient-specific imaging data. *Journal of Medical Devices* 9:030952, 2015.
15. Enriquez-Sarano M, Schaff HV, Orszulak TA, Tajik AJ, Bailey KR, and Frye RL. Valve repair improves the outcome of surgery for mitral regurgitation: a multivariate analysis. *Circulation* 91:1022–1028, 1995. [PubMed: 7850937]
16. Eschenauer HA and Olhoff N. Topology optimization of continuum structures: a review. *Applied Mechanics Reviews* 54:331–390, 2001.
17. Fan R and Sacks MS. Simulation of planar soft tissues using a structural constitutive model: finite element implementation and validation. *Journal of biomechanics* 47:2043–2054, 2014. [PubMed: 24746842]
18. Fung Y.-c. *Biomechanics: mechanical properties of living tissues*, Springer Science & Business Media 2013.
19. Gao H, Feng L, Qi N, Berry C, Griffith BE, and Luo X. A coupled mitral valve-left ventricle model with fluid–structure interaction. *Medical Engineering and Physics* 47:128–136, 2017. [PubMed: 28751011]
20. Goldstein D, Moskowitz AJ, Gelijns AC, Ailawadi G, Parides MK, Perrault LP, Hung JW, Voisine P, Dagenais F, Gillinov AM et al. Two-year outcomes of surgical treatment of severe ischemic mitral regurgitation. *New England Journal of Medicine* 374:344–353, 2016. [PubMed: 26550689]
21. Harb SC and Griffin BP. Mitral valve disease: a comprehensive review. *Current cardiology reports* 19:73, 2017. [PubMed: 28688022]
22. Holda J, Tyrak K, Holda M, Krawczyk-Ozog A, and Klimek-Piotrowska W. Mitral subvalvular apparatus. *Journal of the American College of Cardiology* 71:A1088, 2018.
23. Jassar AS, Brinster CJ, Vergnat M, Robb JD, Eperjesi TJ, Pouch AM, Cheung AT, Weiss SJ, Acker MA, Gorman JH et al. Quantitative mitral valve modeling using real-time three-dimensional echocardiography: technique and repeatability. *The Annals of thoracic surgery* 91:165–171, 2011. [PubMed: 21172507]
24. Kaji S, Nasu M, Yamamuro A, Tanabe K, Nagai K, Tani T, Tamita K, Shiratori K, Kinoshita M, Senda M et al. Annular geometry in patients with chronic ischemic mitral regurgitation. *Circulation* 112:I–409, 2005.
25. Khalighi AH. The mitral valve computational anatomy and geometry analysis.
26. Khalighi AH, Drach A, Bloodworth CH, Pierce EL, Yoganathan AP, Gorman RC, Gorman JH, and Sacks MS. Mitral valve chordae tendineae: topological and geometrical characterization. *Annals of biomedical engineering* 45:378–393, 2017. [PubMed: 27995395]
27. Khalighi AH, Drach A, Gorman RC, Gorman JH, and Sacks MS. Multi-resolution geometric modeling of the mitral heart valve leaflets. *Biomechanics and modeling in mechanobiology* pp. 1–16, 2017.
28. Khalighi AH, Drach A, ter Huurne FM, Lee C-H, Bloodworth C, Pierce EL, Jensen MO, Yoganathan AP, and Sacks MS. A comprehensive framework for the characterization of the complete mitral valve geometry for the development of a population-averaged model In:

- International Conference on Functional Imaging and Modeling of the Heart, pp. 164–171, Springer 2015.
29. Lee C-H, Rabbah J-P, Yoganathan AP, Gorman RC, Gorman JH, and Sacks MS. On the effects of leaflet microstructure and constitutive model on the closing behavior of the mitral valve. *Biomechanics and modeling in mechanobiology* 14:1281–1302, 2015. [PubMed: 25947879]
 30. Mansi T, Voigt I, Georgescu B, Zheng X, Mengue EA, Hackl M, Ionasec RI, Noack T, Seeburger J, and Comaniciu D. An integrated framework for finite-element modeling of mitral valve biomechanics from medical images: application to mitralclip intervention planning. *Medical image analysis* 16:1330–1346, 2012. [PubMed: 22766456]
 31. McCarthy KP, Ring L, and Rana BS. Anatomy of the mitral valve: understanding the mitral valve complex in mitral regurgitation. *European Journal of echocardiography* 11:i3–i9, 2010. [PubMed: 21078837]
 32. Mick SL, Keshavamurthy S, and Gillinov AM. Mitral valve repair versus replacement. *Annals of cardiothoracic surgery* 4:230, 2015. [PubMed: 26309824]
 33. Morgan AE, Pantoja JL, Weinsaft J, Grossi E, Guccione JM, Ge L, and Ratcliffe M. Finite element modeling of mitral valve repair. *Journal of biomechanical engineering* 138:021009, 2016. [PubMed: 26632260]
 34. Mozaffarian D, Benjamin EJ, Go AS, Arnett DK, Blaha MJ, Cushman M, Das SR, de Ferranti S, Després J-P, Fullerton HJ et al. Heart disease and stroke statistics 2016 update: a report from the American Heart Association. *Circulation* 133:e38–e360, 2016. [PubMed: 26673558]
 35. Obadia JF, Casali C, Chassignolle JF, and Janier M. Mitral subvalvular apparatus: different functions of primary and secondary chordae. *Circulation* 96:3124–3128, 1997. [PubMed: 9386184]
 36. Pham T, Kong F, Martin C, Wang Q, Primiano C, McKay R, Elefteriades J, and Sun W. Finite element analysis of patient-specific mitral valve with mitral regurgitation. *Cardiovascular engineering and technology* 8:3–16, 2017. [PubMed: 28070866]
 37. Pouch AM, Xu C, Yushkevich PA, Jassar AS, Vergnat M, Gorman JH, Gorman RC, Sehgal CM, and Jackson BM. Semi-automated mitral valve morphometry and computational stress analysis using 3d ultrasound. *Journal of biomechanics* 45:903–907, 2012. [PubMed: 22281408]
 38. Prot V, Haaverstad R, and Skallerud B. Finite element analysis of the mitral apparatus: annulus shape effect and chordal force distribution. *Biomechanics and modeling in mechanobiology* 8:43–55, 2009. [PubMed: 18193309]
 39. Prot V, Skallerud B, Sommer G, and Holzapfel GA. On modelling and analysis of healthy and pathological human mitral valves: two case studies. *Journal of the mechanical behavior of biomedical materials* 3:167–177, 2010. [PubMed: 20129416]
 40. Rausch MK, Famaey N, Shultz TO, Bothe W, Miller DC, and Kuhl E. Mechanics of the mitral valve. *Biomechanics and modeling in mechanobiology* 12:1053–1071, 2013. [PubMed: 23263365]
 41. Redaelli A A model of health: Mathematical modeling tools play an important role in optimizing new treatment options for heart disease. *IEEE pulse* 6:27–32, 2015.
 42. Rego BV, Ayoub S, Khalighi AH, Drach A, Gorman R, Gorman J, and Sacks MS. Alterations in mechanical properties and in vivo geometry of the mitral valve following myocardial infarction. In: *Proceedings of the 2017 Summer Biomechanics, Bioengineering and Biotransport Conference*, pp SB3C2017–1 Google Scholar. 2017.
 43. Rego BV and Sacks MS. A functionally graded material model for the transmural stress distribution of the aortic valve leaflet. *Journal of biomechanics* 54:88–95, 2017. [PubMed: 28256242]
 44. Rego BV, Wells SM, Lee C-H, and Sacks MS. Mitral valve leaflet remodeling during pregnancy: insights into cell-mediated recovery of tissue homeostasis. *Journal of The Royal Society Interface* 13:20160709, 2016.
 45. Rim Y, McPherson DD, Chandran KB, and Kim H. The effect of patient-specific annular motion on dynamic simulation of mitral valve function. *Journal of biomechanics* 46:1104–1112, 2013. [PubMed: 23433464]

46. Ritchie J, Jimenez J, He Z, Sacks MS, and Yoganathan AP. The material properties of the native porcine mitral valve chordae tendineae: an in vitro investigation. *Journal of biomechanics* 39:1129–1135, 2006. [PubMed: 16549101]
47. Rozenberg G and Salomaa A. *The mathematical theory of L systems*, volume 90, Academic press 1980.
48. Sacks MS, Khalighi A, Rego B, Ayoub S, and Drach A. On the need for multi-scale geometric modelling of the mitral heart valve.
49. Sacks MS, Smith DB, and Hiester ED. A small angle light scattering device for planar connective tissue microstructural analysis. *Annals of biomedical engineering* 25:678–689, 1997. [PubMed: 9236980]
50. Sand M, Naftel D, Blackstone E, Kirklin J, and Karp R. A comparison of repair and replacement for mitral valve incompetence. *The Journal of thoracic and cardiovascular surgery* 94:208–219, 1987. [PubMed: 3613619]
51. Smith PK, Puskas JD, Ascheim DD, Voisine P, Gelijns AC, Moskowitz AJ, Hung JW, Parides MK, Ailawadi G, Perrault LP et al. Surgical treatment of moderate ischemic mitral regurgitation. *New England Journal of Medicine* 371:2178–2188, 2014. [PubMed: 25405390]
52. Stevanella M, Maffessanti F, Conti CA, Votta E, Arnoldi A, Lombardi M, Parodi O, Caiani EG, and Redaelli A. Mitral valve patient-specific finite element modeling from cardiac mri: application to an annuloplasty procedure. *Cardiovascular Engineering and Technology* 2:66–76, 2011.
53. Sturla F, Onorati F, Votta E, Pechlivanidis K, Stevanella M, Milano AD, Puppini G, Mazzucco A, Redaelli A, and Faggian G. Is it possible to assess the best mitral valve repair in the individual patient? preliminary results of a finite element study from magnetic resonance imaging data. *The Journal of thoracic and cardiovascular surgery* 148:1025–1034, 2014. [PubMed: 25052823]
54. Sun W, Martin C, and Pham T. Computational modeling of cardiac valve function and intervention. *Annual review of biomedical engineering* 16:53–76, 2014.
55. Trichon BH, Felker GM, Shaw LK, Cabell CH, and OConnor CM. Relation of frequency and severity of mitral regurgitation to survival among patients with left ventricular systolic dysfunction and heart failure. *American Journal of Cardiology* 91:538–543, 2003. [PubMed: 12615256]
56. Wenk JF, Zhang Z, Cheng G, Malhotra D, Acevedo-Bolton G, Burger M, Suzuki T, Saloner DA, Wallace AW, Guccione JM et al. First finite element model of the left ventricle with mitral valve: insights into ischemic mitral regurgitation. *The Annals of thoracic surgery* 89:1546–1553, 2010. [PubMed: 20417775]
57. Yun K and Miller D. Mitral valve repair versus replacement. *Cardiology clinics* 9:315–327, 1991. [PubMed: 2054820]
58. Zhang F, Kanik J, Mansi T, Voigt I, Sharma P, Ionasec RI, Subrahmanyam L, Lin BA, Sugeng L, Yuh D et al. Towards patient-specific modeling of mitral valve repair: 3d transesophageal echocardiography-derived parameter estimation. *Medical image analysis* 35:599–609, 2017. [PubMed: 27718462]
59. Zhang W, Ayoub S, Liao J, and Sacks MS. A meso-scale layer-specific structural constitutive model of the mitral heart valve leaflets. *Acta biomaterialia* 32:238–255, 2016. [PubMed: 26712602]

(a) Ground Truth CT anatomy**(b) 3D Echocardiography****Figure 1:**

A representative MVCT is shown (a) [adapted from Khalighi et al.²⁶] While echocardiography has improved significantly in recent years (b), it still cannot fully capture the thin intricate structure of MV chordal constituents.

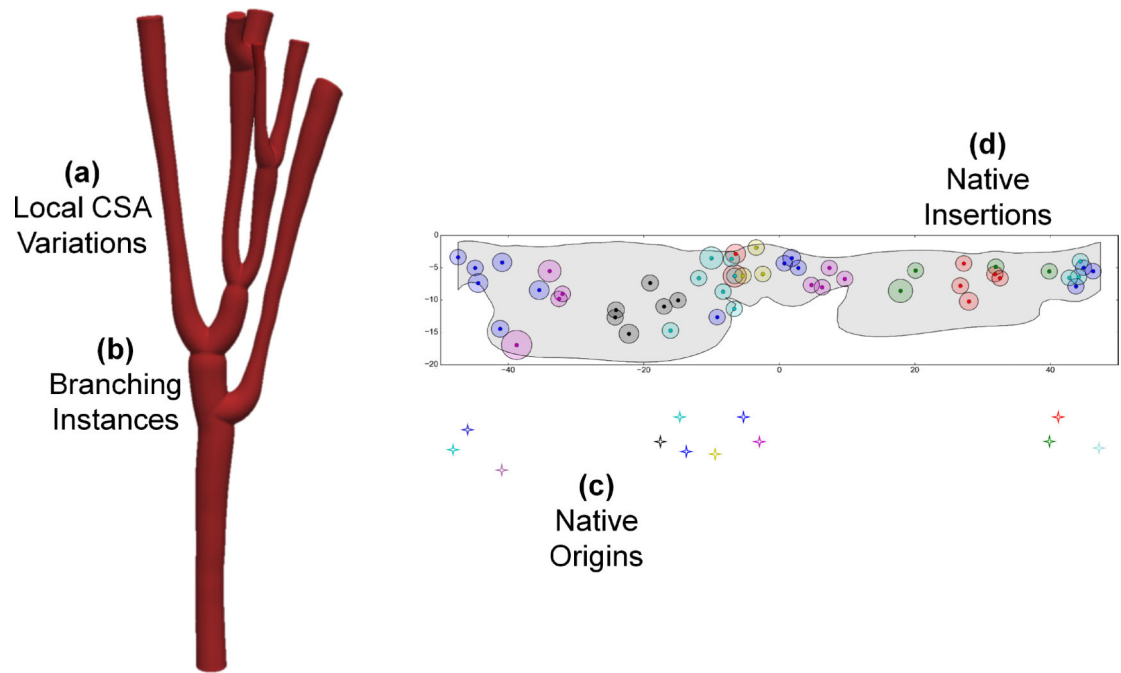


Figure 2:

The anatomical features of native MVCT are shown for a representative chord. The real chordal anatomy is quite complex as a result of (a) area variations, (b) numerous branching instances, and the scatter of native chordal (c) origins and (d) insertions. Notably, these features are also missing in the clinical imaging data

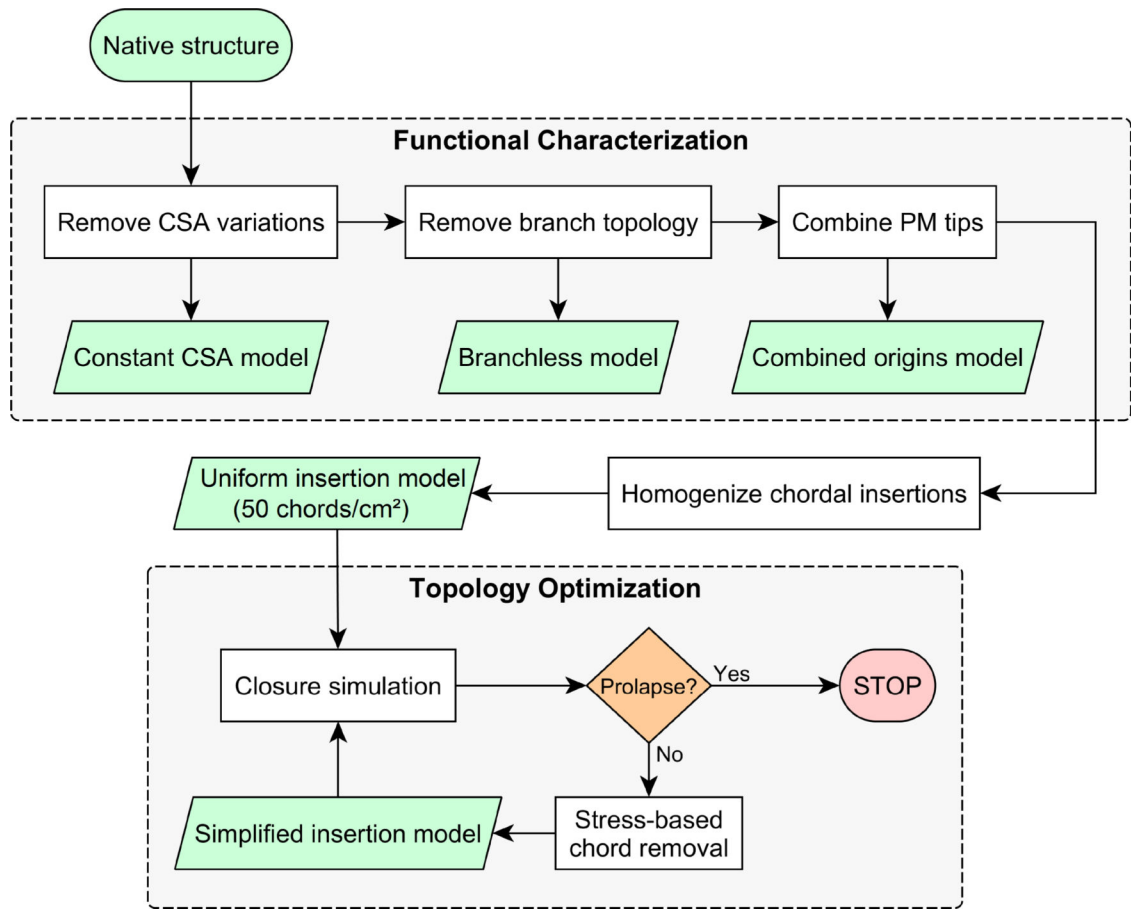


Figure 3: We systematically simplified the structure of native chordal anatomy to perform a functional characterization of the MVCT and, in turn, elucidate the structure-function relation of the chordal features unresolvable via clinical imaging. Further, we sought to build functionally equivalent MVCT models that are geometrically simple in a topology optimization framework

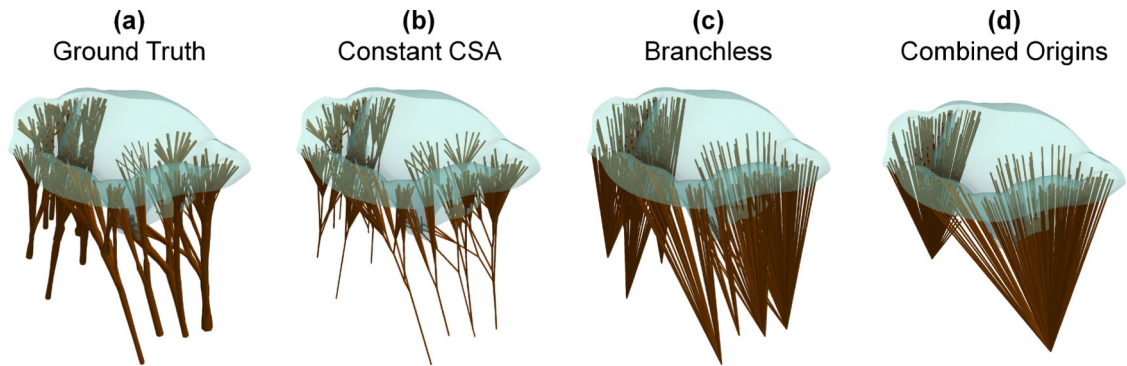


Figure 4:

Starting from the ground truth model with native MVCT (a), we eliminated area variations (b) to analyze the impact of local thickness variations on FE model development. Then, the “constant CSA” model was further simplified by removing all the internal branching points (c) and consecutively combining the chordal origin locations (d). This ensemble of models allowed us to study the functional impact of the native chordal anatomic features except the chordal insertions.

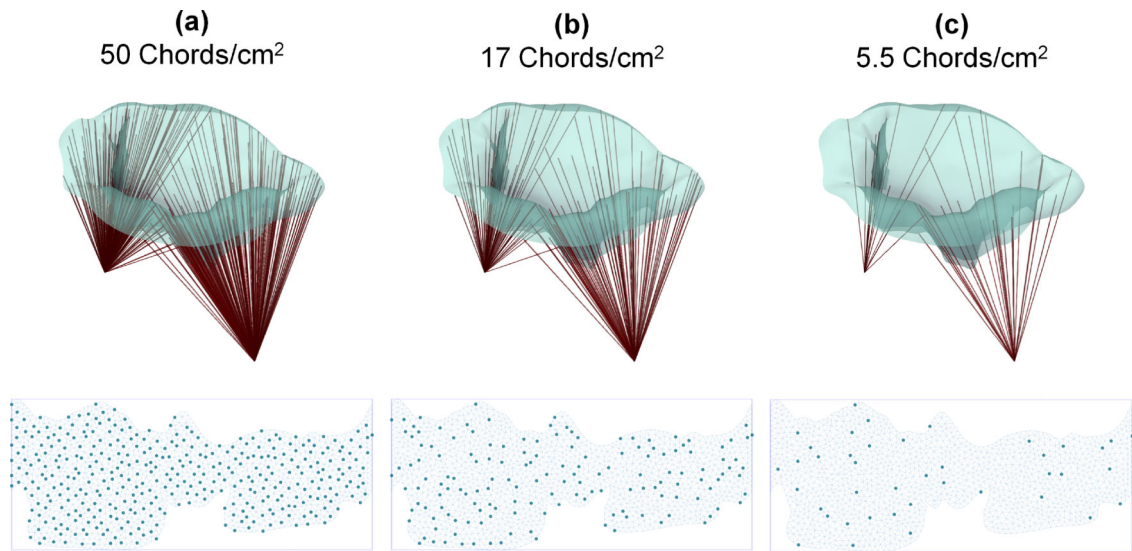


Figure 5:

To analyze the effect of native insertion locations, we homogenized the insertion map of the native chordal structure and developed a synthetic model with the same density of chords distributed uniformly (a). This model was then systematically simplified in a topology optimization framework (b) to investigate the least of number of chordal strands required to mimic the response of ground truth model till the onset of prolapse due to lack of sufficient support on the leaflet from the synthetic MVCT models (c)

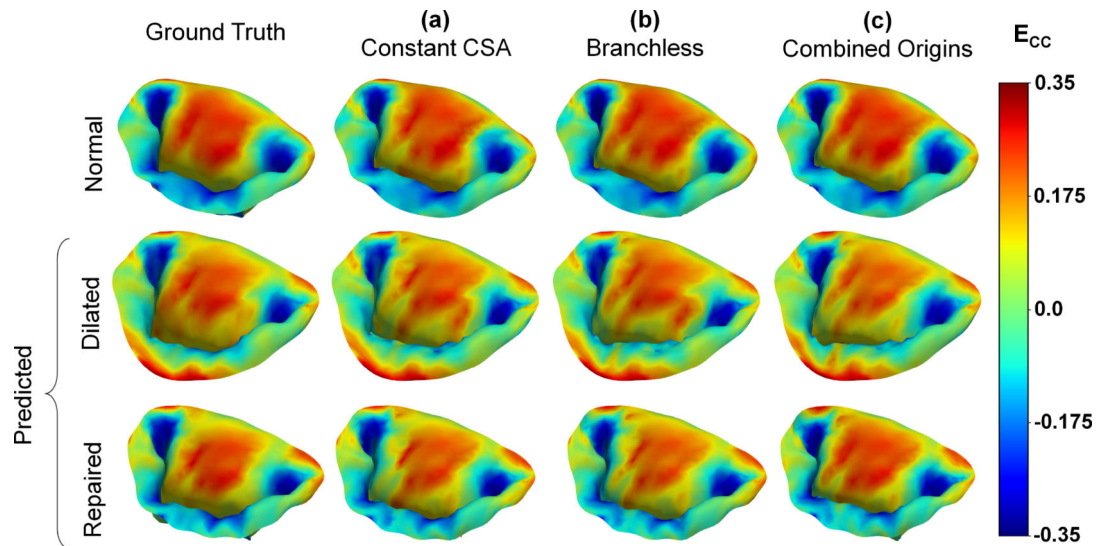


Figure 6:

Interestingly, the result of MVCT functional characterization demonstrates that carefully calibrated models with simplified chordal anatomy can be developed while preserving the predictive power. The comparison of models with no CSA variations (a), branching patterns (b), and origins scatter (c) with the ground truth models shows minimal discrepancies in prediction of shape as well as the strain and stress tensors. For brevity, only circumferential strain (E_{cc}) results are shown here.

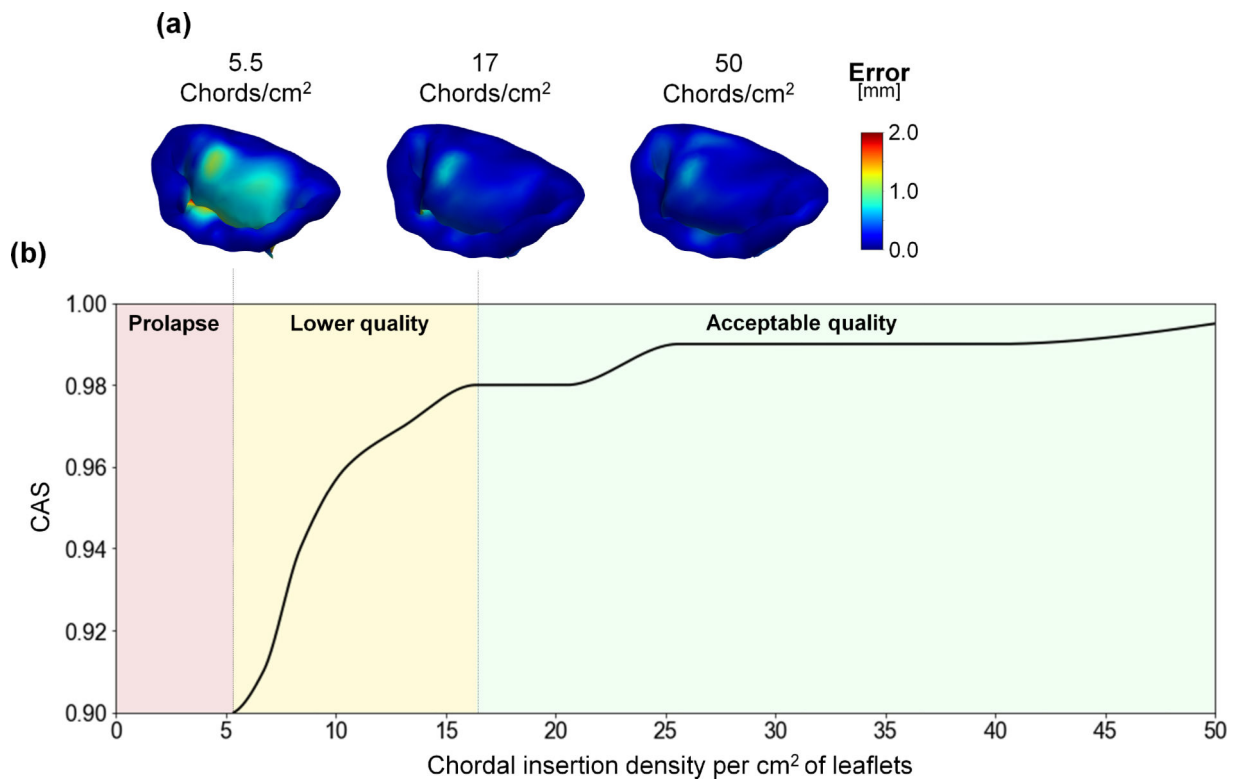


Figure 7:

A minimum density of chords are required to ensure the MVCT models can be properly calibrated to the normal condition (a). In terms of overall model performance, the rate of decay in accuracy score (b) implies that certain regimes of model quality exist. This behavior strongly suggest that geometrically simple, functionally equivalent models can be efficiently developed and calibrated to reproduce the effect of native MVCT on MV function

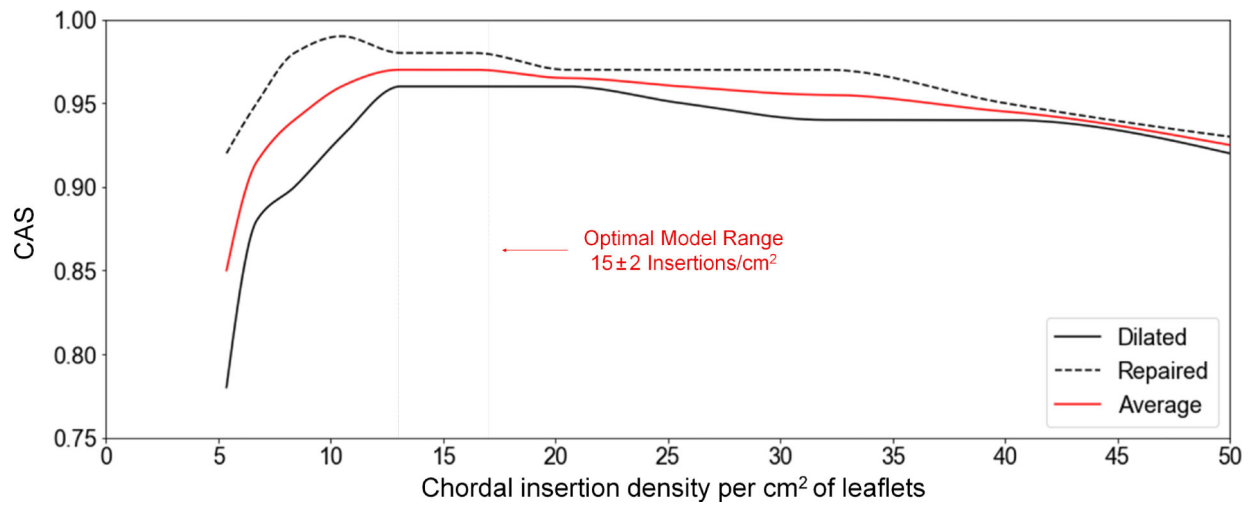


Figure 8:

The quality of MV closure predictions based on simplified MVCT models indicates that optimal MVCT models can be developed. While removing too many chords renders the MVCT models incompetent, the models with more than adequate density of chords, above 23 insertions/cm², are essentially over-fitting the normal calibration conditions and thus perform suboptimally in predicting altered states.

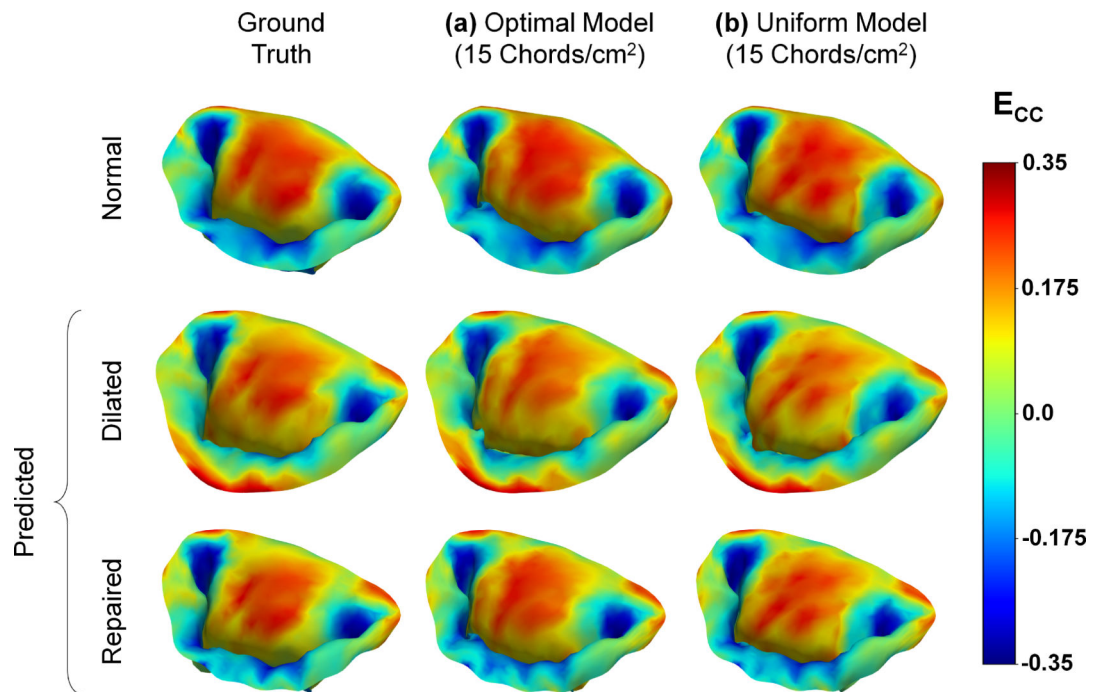


Figure 9:

In addition to developing functionally equivalent models through topology optimization (a), we tested even a more simplified model with a uniform map of insertion locations with the optimal density (b). The results show that the developed uniform MVCT model can achieve high accuracy in predicting MV closure compared to the ground truth simulations. Remarkably, no knowledge of the native chordal anatomy is required to build and calibrate this model (b).

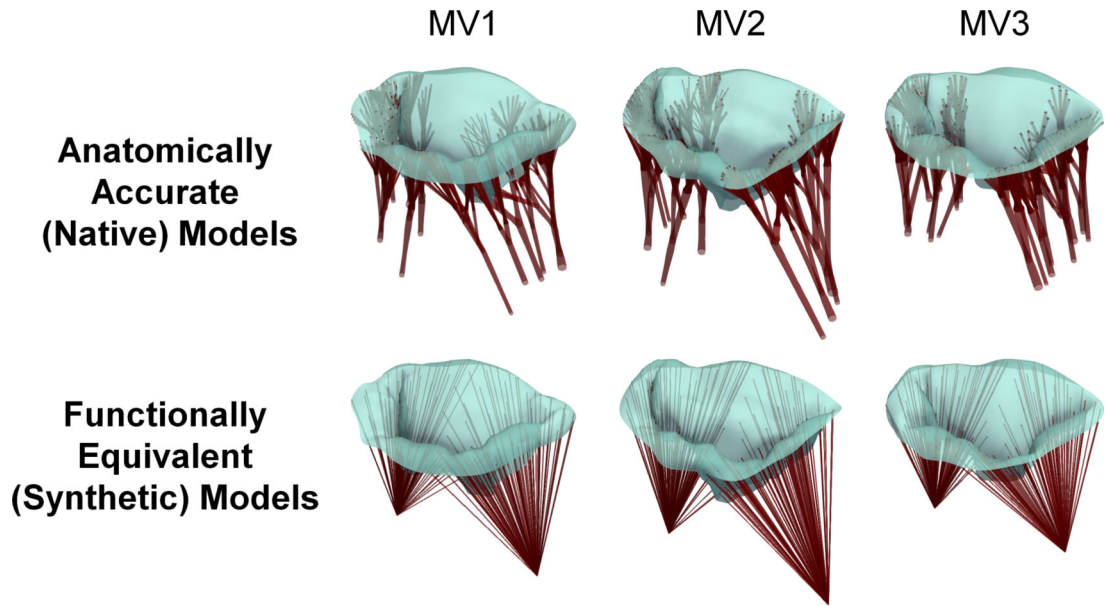


Figure 10:

The study was performed on 3 specimens to reproduce the results of functionally equivalent models of the MVCT on multiple valves.

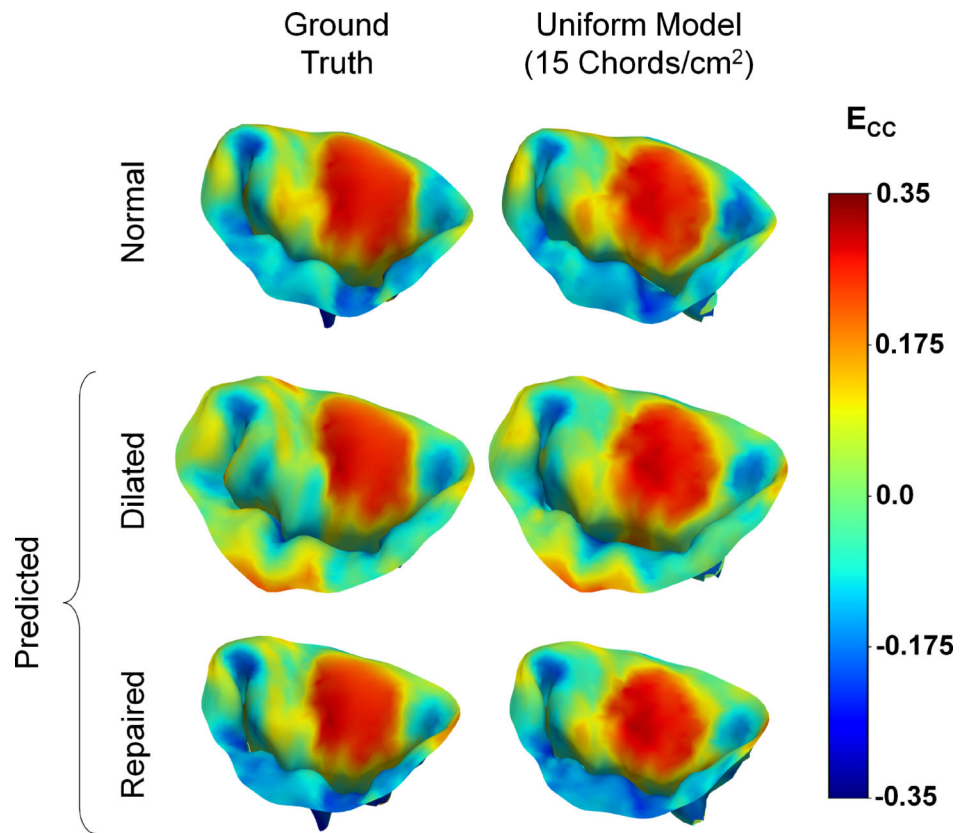


Figure 11: Closure simulations of MV2 are shown for a functionally equivalent MVCT and the ground truth models.

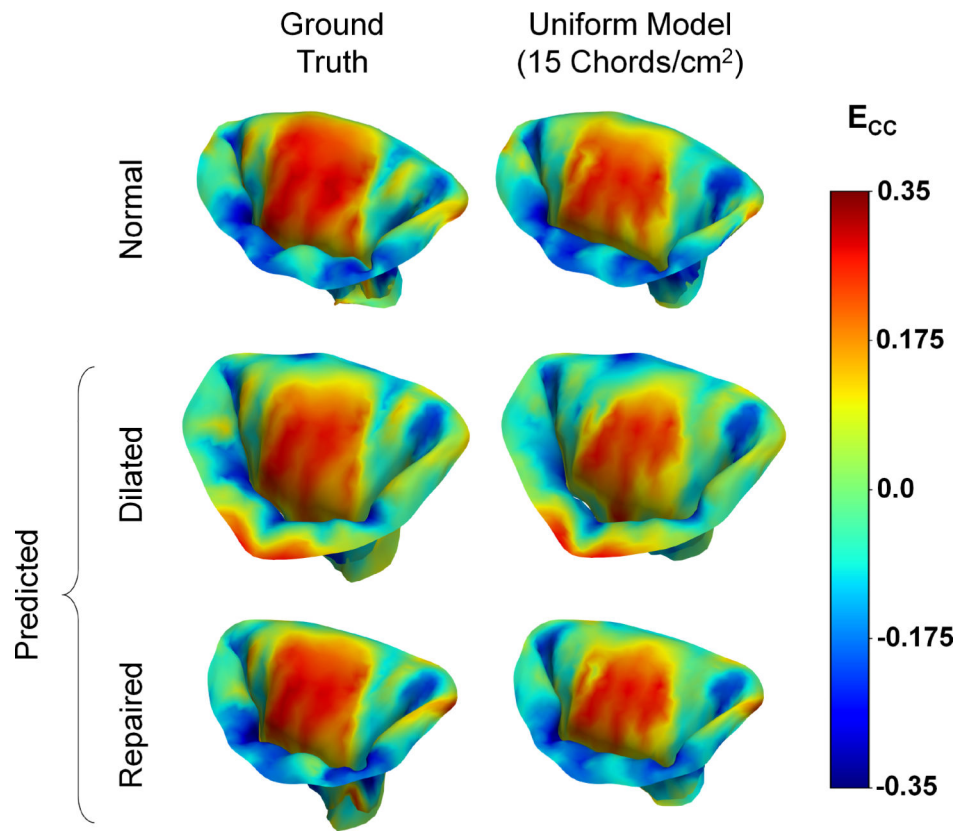


Figure 12: Closure simulations of MV3 are shown for a functionally equivalent MVCT and the ground truth models.

Table 1:

CAS scores for 3 valves studied in this work using functionally equivalent MVCT models

	MV1	MV2	MV3
Normal	0.98	0.95	0.95
Dilated	0.95	0.92	0.94
Repaired	0.97	0.95	0.93

Author Manuscript

Author Manuscript

Author Manuscript

Author Manuscript